IOP Publishing Journal of Geophysics and Engineering

J. Geophys. Eng. 15 (2018) 1663–1672 (10pp) https://doi.org/10.1088/1742-2140/aabf1d

Seismic data analysis using synchrosqueezing short time Fourier transform

Guoning Wu[1] and **Yatong Zhou**[2,3]

[1] College of Science, China University of Petroleum-Beijing, Beijing, People's Republic of China
[2] School of Electronic and Information Engineering, Hebei University of Technology, Tianjin, People's Republic of China

E-mail: zyt@hebut.edu.cn

Received 13 December 2017, revised 9 April 2018
Accepted for publication 18 April 2018
Published 16 May 2018

Abstract

The synchrosqueezing wavelet transform (SWT) reallocates the wavelet transform values to different points, hence produces a sharp spectral decomposition for the input signal. The SWT method was widely used for de-noising, spectral decomposition, etc. In this paper, a new synchrosqueezing method was proposed based on short time Fourier transform. The proposed method reassigns the short time Fourier transform values to different points, thus produces a concentrated time–frequency map. Furthermore, the proposed method has an inverse formula, which allows the reconstruction of the input signal from its spectral decomposition. Examples showed that the proposed method is effective for revealing the time–frequency characterizations of non-stationary signals.

Keywords: time–frequency analysis, synchrosqueezing method, short time Fourier transform

(Some figures may appear in colour only in the online journal)

Introduction

Time–frequency distribution is a powerful tool for non-stationary signal analysis, which was widely used in seismic data interpretation (Castagna *et al* 2003, Reine *et al* 2009, Chen *et al* 2014, Liu *et al* 2016). Conventional time–frequency methods are either 'linear' or 'quadratic'. For example, short time Fourier transform (STFT) (Cohen 1989), wavelet transform (WT) (Mallat 1989), and S-transform (ST) (Stockwell *et al* 1996), are linear. These linear methods pick up sections of the input signal with windows moving along the time axis. The linear methods were widely used in wide range of applications, however, the Fourier transform of the windowed section usually generates spurious frequencies, and these frequencies make the true time–frequency map unclear (Tary *et al* 2014). The Wigner–Ville transform and its variants, such as the Cohen class are quadratic. Quadratic methods produce interference terms and make the time–frequency densities negative, thus generate misleading results. Furthermore, the inversions for the quadratic methods are less straightforward (Daubechies *et al* 2011, Huang *et al* 2015).

The empirical mode decomposition (EMD) (Huang *et al* 1998), was introduced in the late 1990s, aims to extract symmetric, narrow-band waveforms called intrinsic mode functions (IMF) in a data-driven manner. The EMD method was widely used in signal processing. However, the EMD suffers from mode mixing and splitting problems. In order to solve the above problems, alternative methods were proposed based on EMD such as ensemble EMD (EEMD) (Wu and Huang 2009), and complete ensemble empirical decomposition (CEEMD) (Torres *et al* 2011). In spite of its usefulness in a wide range of applications, the EMD method and its variants lack firm mathematical foundations. The synchrosqueezing wavelet transform (SWT) was recently proposed (Daubechies *et al* 2011), with a rigorous theoretical foundation, this method captures the philosophy of the EMD method but uses a different method to construct its IMF. Auger *et al* (2013) showed the SWT can be viewed as a reassignment method, this method sharpens the time–frequency map of the wavelet transform by reallocating its values to different points. Herrera *et al* (2014), Chen *et al* (2014) applied the SWT method to seismic data analysis. Synchrosqueezing method can be used by many classical time–frequency methods in order to get concentrated time–frequency

[3] Author to whom any correspondence should be addressed.

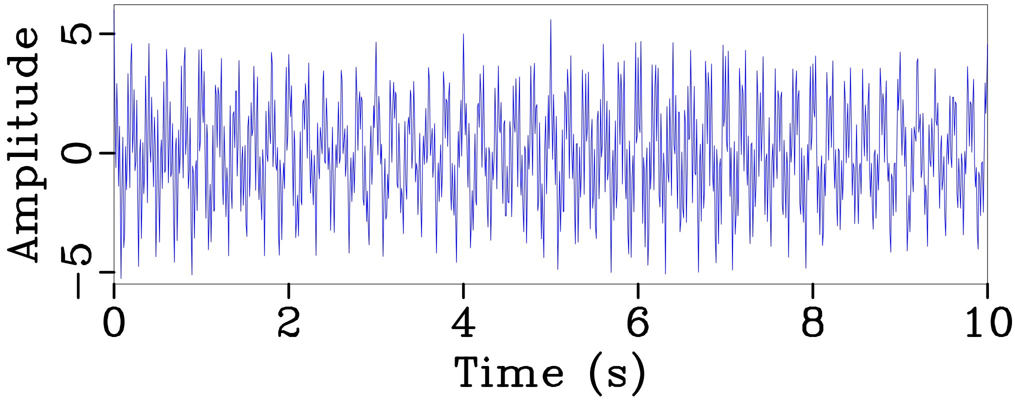

Figure 1. Synthetic signal.

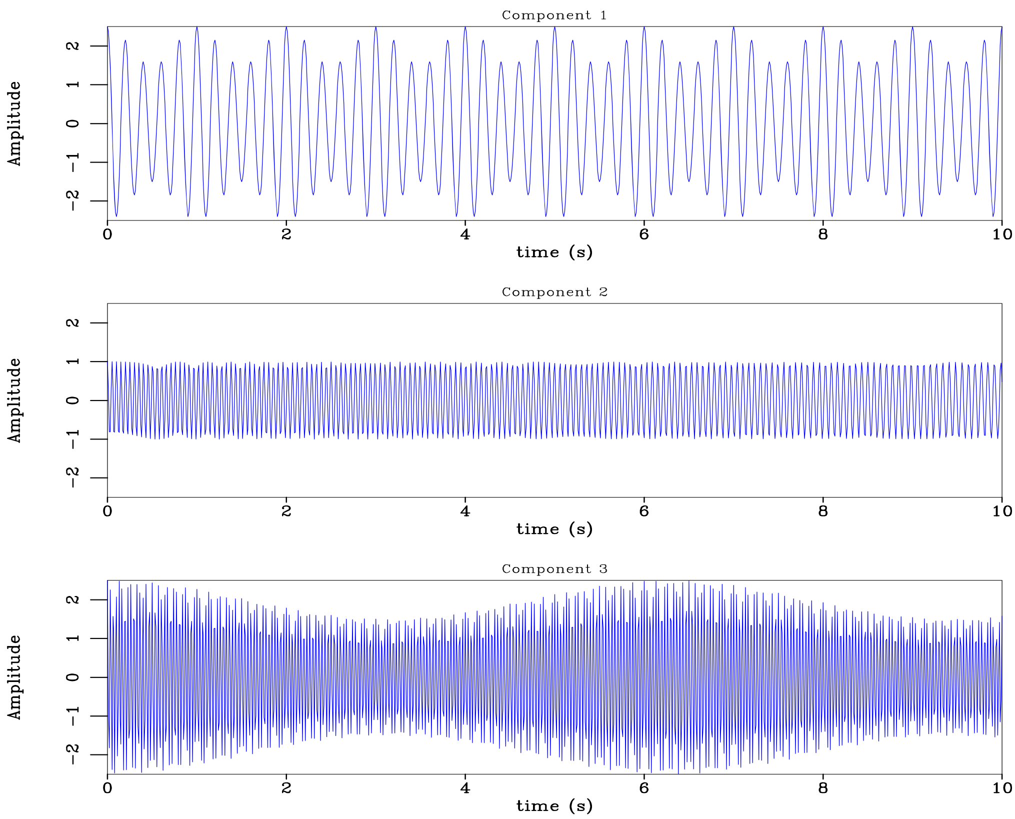

Figure 2. Components of the synthetic signal of figure 1.

representations. For example, the synchrosqueezing S-transform (Huang *et al* 2016, 2017), the matching synchrosqueezing wavelet transform (Wang *et al* 2016), the nonlinear squeezing time–frequency transform (Wang *et al* 2015), and the second-order synchrosqueezing transform (Oberlin *et al* 2015), synchrosqueezing method also be used as filter banks, subsampling and processing (Holighaus *et al* 2016).

The spectrogram can be viewed as a variation of the Wigner–Ville distribution (Auger *et al* 2013). The energies spread over the instantaneous frequencies due to the windowing process. In order to get a concentrated time–frequency map, Auger and Flandrin (1995) proposed the reassignment method, which reallocates its values to different points. Auger *et al* (2012) also presented a new Levenberg–Marquardt method, which makes the reassignment method adjustable. The synchrosqueezing method with the advantage of inversion has received new attention (Oberlin *et al* 2014).

In this paper, a new time–frequency method named synchrosqueezing short time Fourier transform (SSTFT) was proposed. The proposed method is a combination of the STFT and the synchrosqueezing method. The synchrosqueezing process squeezes the energies of STFT to the instantaneous frequencies and therefore generates a concentrated time–frequency map (Mallat 2009). Firstly, the forward and inverse transforms were given. The proofs of the forward and inverse transforms are different from those of Oberlin *et al* (2014), but similar to the proofs of Daubechies *et al* (2011) and Huang *et al* (2016). Numerical results showed that the proposed method is effective

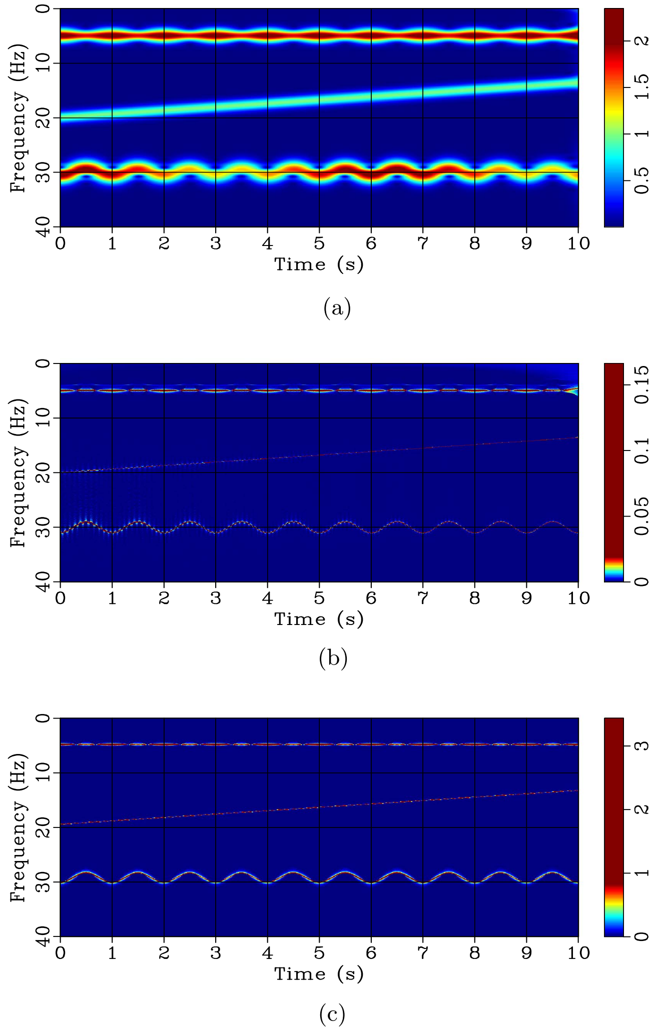

Figure 3. Time–frequency map for the synthetic signal of figure 1: (a) time–frequency map using local attribute. (b) Time–frequency map using SWT, with a 64-point length Morlet wavelet. (c) Time–frequency map using SSTFT, with a 64-point length Gaussian window.

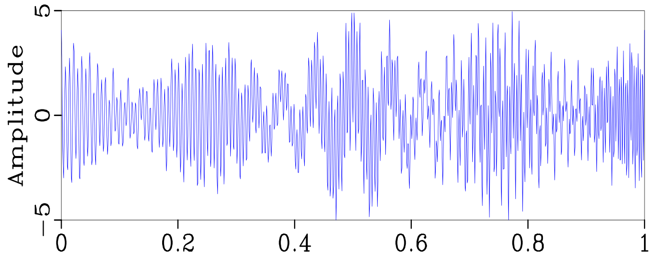

Figure 4. Synthetic signal.

for revealing the characterizations of non-stationary signals. Finally, the proposed method was used for seismic data interpretation.

Theorem

Synchrosqueezing short time Fourier transform (SSTFT)

The SWT was used to analyze a wide variety of signals. The appendix gives a short introduction to the SWT algorithm.

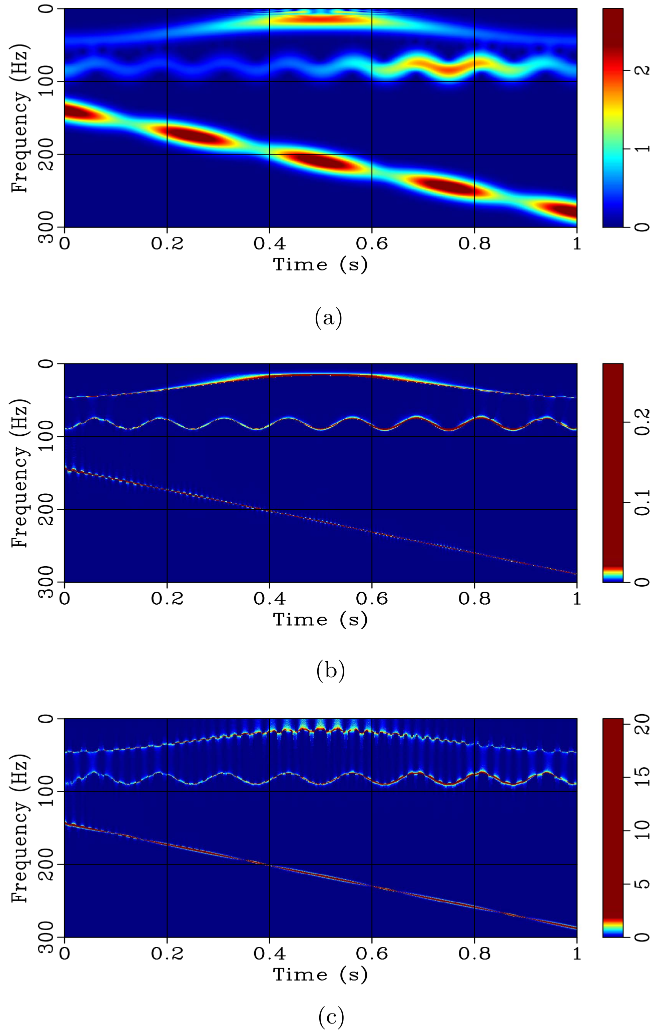

Figure 5. Time–frequency map for the synthetic signal of figure 4: (a) time–frequency map using local attribute. (b) Time–frequency map using SWT, with a 64-point length Morlet wavelet. (c) Time–frequency map using SSTFT, with a 64-point length Gaussian window.

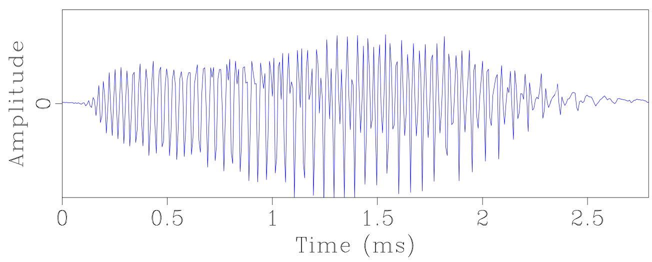

Figure 6. Bat signal.

For its concentration property, the synchrosqueezing method was used by other transforms to generate concentrated time–frequency representations. For example the synchrosqueezing S-transform (Huang *et al* 2016, 2017). In the following, the synchrosqueezing method is used to sharpen the STFT map, and therefore, generates a concentrated time–frequency map named SSTFT.

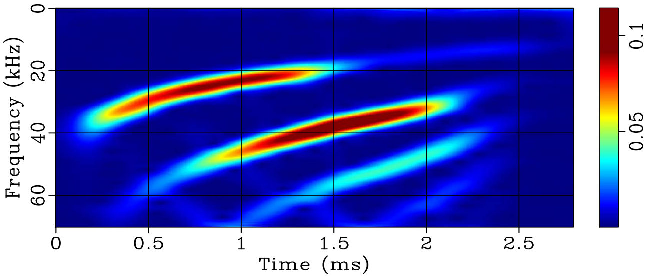

(a)

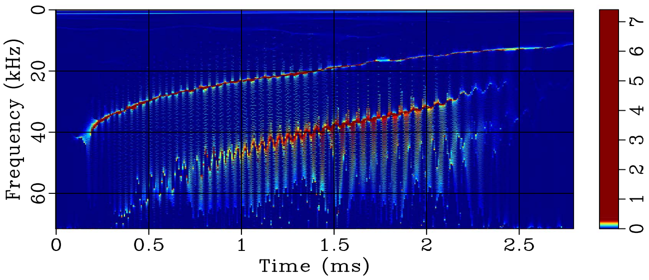

(b)

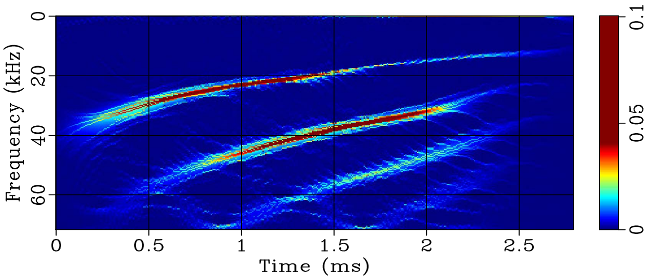

(c)

Figure 7. Time–frequency map for the bat signal of figure 6: (a) time–frequency map using short time Fourier transform, with a 64-point length Gaussian window. (b) Time–frequency map using Oberlin's method, with a 64-point length Gaussian window. (c) Time–frequency map using SSTFT, with a 64-point length Gaussian window.

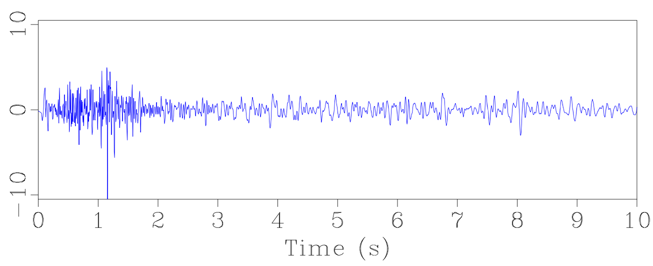

Figure 8. A trace from a marine survey.

The forward SSTFT

The STFT of a signal $x(t)$ is (Auger *et al* 2013)

$$W_x(\omega,\,\tau) = \mathrm{e}^{-\mathrm{i}\omega\tau}\int_{-\infty}^{\infty} x(t)\overline{g(t-\tau)}\mathrm{e}^{-\mathrm{i}\omega(t-\tau)}\,\mathrm{d}t, \qquad (1)$$

where $\overline{g(t-\tau)}$ is the complex conjugate of the window function $g(t-\tau)$, ω is the angular frequency, t is the time and τ is the time translation. Let $G(t,\ \omega) = g(t)\mathrm{e}^{\mathrm{i}\omega t}$, then

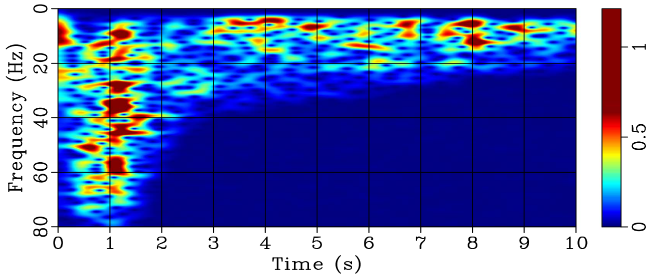

(a)

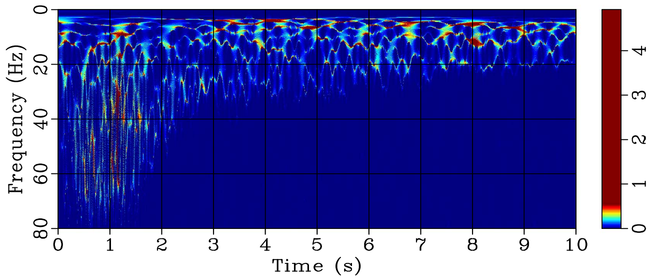

(b)

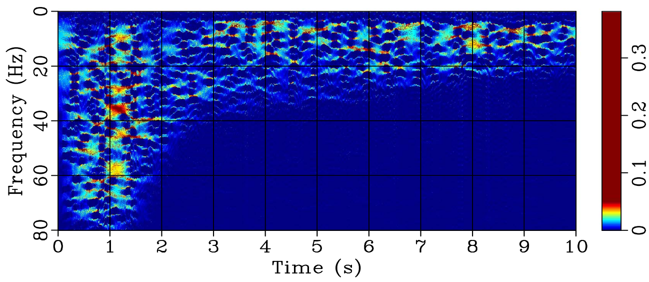

(c)

Figure 9. Time–frequency map for the trace of figure 8: (a) time–frequency map using local attribute. (b) Time–frequency map using SWT, with a 64-point Morlet Wavelet. (c) Time–frequency map using SSTFT, with a 64-point Gaussian window.

equation (1) can be rewritten as

$$W_x(\omega,\,\tau) = \mathrm{e}^{-\mathrm{i}\omega\tau}\int_{-\infty}^{\infty} x(t)\overline{G(t-\tau,\,\omega)}\,\mathrm{d}t. \qquad (2)$$

The spectrogram is $\|W_x(\omega,\,\tau)\|^2$, which can be viewed as the 2D smoothing of the Wigner–Ville distribution of the analyzed signal by the Wigner–Ville distribution of the analyzing window (Auger *et al* 2013). The smoothing process will decrease the resolution of STFT. For example a sinusoidal $f(t) = \mathrm{e}^{\mathrm{i}\xi_0 t}$, the Fourier transform of which is the Dirac $\hat{f}(\omega) = 2\pi\delta(\omega-\xi_0)$, has a STFT (Mallat 2009):

$$W_f(\omega,\,\tau) = \hat{g}(\omega-\xi_0)\mathrm{e}^{-\mathrm{i}\tau(\omega-\xi_0)}. \qquad (3)$$

For the STFT of the sinusoidal function, its energies are spread over the interval $[\xi_0-\sigma_{\frac{\omega}{2}},\ \xi_0+\sigma_{\frac{\omega}{2}}]$, where $\sigma_{\frac{\omega}{2}}$ is the standard deviation of the function $\hat{g}(\omega)$. Whereas, the STFT of a Dirac function $f(t) = \delta(t-u_0)$ is

$$W_f(\omega,\,\tau) = g(u_0-\tau)\mathrm{e}^{-\mathrm{i}\omega u_0}. \qquad (4)$$

For the Dirac function mentioned above, its energies are spread over in the time interval $[u_0-\sigma_{\frac{t}{2}},\ u_0+\sigma_{\frac{t}{2}}]$, where $\sigma_{\frac{t}{2}}$ is the standard deviation of the of the function $g(u)$

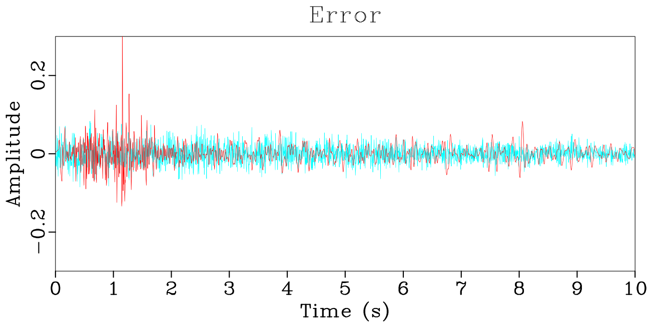

Figure 10. Reconstruction errors of SWT (the blue line) and SSTFT (the red line) for the trace of figure 8.

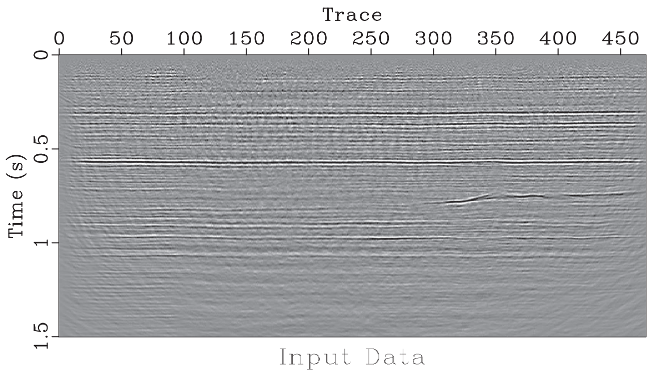

Figure 11. Real seismic data.

In order to improve the time–frequency resolution, the synchrosqueezing method was used with the STFT to generate a concentrated time–frequency representation. Similar to the SWT, for any $W_x(\omega, \tau) \neq 0$, a candidate instantaneous frequency for the signal x is following. According to Plancherel's theorem, equation (2) can be written as

$$W_x(\omega, \tau) = \frac{1}{2\pi} e^{-i\omega\tau} \int_{-\infty}^{\infty} \hat{x}(\xi) \overline{\hat{g}(\xi - \omega)} e^{i\xi\tau} \, d\xi, \tag{5}$$

where ξ is the angular frequency, $\hat{x}(\xi)$ is the Fourier transform of $x(t)$, $\hat{g}(\xi)$ is the Fourier transform of g. To motivate the idea, let $x(t) = A\cos(\omega_0 t)$, its Fourier transform is

$$\hat{x}(\xi) = A\pi[\delta(\xi - \omega_0) + \delta(\xi + \omega_0)]. \tag{6}$$

Take a window g that is concentrated on the positive frequency axis: $\widehat{g(\xi)} = 0$ for $\xi < 0$. Substituting equation (6) into (5) yields

$$W_x(\omega, \tau) = \frac{A}{2} \overline{\hat{g}(\omega_0 - \omega)} e^{-i(\omega - \omega_0)\tau}. \tag{7}$$

For any (ω, τ) with $W_x(\omega, \tau) \neq 0$, a candidate instantaneous frequency $\widetilde{\omega}_x(\omega, \tau)$ for the signal x can be computed by

$$\widetilde{\omega}_x(\omega, \tau) = -i(W_x(\omega, \tau))^{-1} \frac{\partial}{\partial \tau}(W_x(\omega, \tau)) + \omega. \tag{8}$$

If the frequency variables ω, $\widetilde{\omega}$ are discretized i.e. $W_x(\omega, \tau)$ was computed only at discrete value ω_k, where $\omega_k - \omega_{k-1} = (\Delta\, \omega)_k$ The SSTFT is given by

$$SW_x(\widetilde{\omega}_l, \tau) = (\Delta\widetilde{\omega})^{-1} \sum_{\omega_k : |\widetilde{\omega}(\omega_k, \tau) - \widetilde{\omega}_l| \leqslant \Delta\widetilde{\omega}/2} W_x(\omega_k, \tau) e^{i\omega_k \tau} (\Delta\omega)_k. \tag{9}$$

This is the forward transform. The energies of the STFT be squeezed to the instantaneous frequencies locations according to the equation (9) in order to get a concentrated time–frequency representation. The SSTFT is a combination of the STFT and the synchrosqueezing method.

The inverse SSTFT

The following argument shows that the signal can be reconstructed.

$$\begin{aligned}
&\int_{-\infty}^{+\infty} W_x(\omega, \tau) e^{i\omega\tau} \, d\omega \\
&= \int_{-\infty}^{+\infty} \int_{-\infty}^{+\infty} x(t) \overline{g(t - \tau)} e^{-i\omega t} e^{i\omega\tau} \, d\omega \, dt \\
&= \int_{-\infty}^{+\infty} \left(\int_{-\infty}^{+\infty} x(t) \overline{g(t - \tau) e^{i\omega t}} \, dt \right) e^{i\omega\tau} \, d\omega \\
&= \int_{-\infty}^{+\infty} \left(\frac{1}{2\pi} \int_{-\infty}^{+\infty} \hat{x}(\xi) \overline{\hat{g}(\xi - \omega) e^{-i(\xi - \omega)\tau}} \, d\xi \right) e^{i\omega\tau} \, d\omega \\
&= \frac{1}{2\pi} \int_{-\infty}^{+\infty} \hat{x}(\xi) e^{i\xi\tau} \, d\xi \int_{-\infty}^{+\infty} \overline{\hat{g}(\xi - \omega)} \, d\omega \\
&= \frac{1}{2\pi} \int_{-\infty}^{+\infty} \hat{x}(\xi) e^{i\xi\tau} \, d\xi \int_{-\infty}^{+\infty} \overline{\hat{g}(\omega)} \, d\omega \\
&= x(\tau) \int_{-\infty}^{+\infty} \overline{\hat{g}(\omega)} \, d\omega.
\end{aligned} \tag{10}$$

Suppose the window function is real, we derive that $\hat{g}(-\omega) = \overline{\hat{g}(\omega)}$. Equation (10) can be written as

$$\begin{aligned}
&\int_{-\infty}^{+\infty} W_x(\omega, \tau) e^{i\omega\tau} \, d\omega \\
&= x(\tau) \int_{-\infty}^{+\infty} \overline{\hat{g}(\omega)} \, d\omega \\
&= x(\tau) \int_{0}^{+\infty} \hat{g}(\omega) + \overline{\hat{g}(\omega)} \, d\omega \\
&= x(\tau) \int_{0}^{+\infty} 2\Re(\hat{g}(\omega)) d\omega.
\end{aligned} \tag{11}$$

If we let $E_g = \int_{-\infty}^{+\infty} \overline{\hat{g}(\omega)} \, d\omega$, the signal can be reconstructed by

$$x(\tau) = (E_g)^{-1} \int_{-\infty}^{\infty} W_x(\omega, \tau) e^{i\omega\tau} \, d\omega. \tag{12}$$

The following is the discrete reconstruction formula. From equations (9) and (12) we have

$$\begin{aligned}
x(\tau) &\approx (E_g)^{-1} \sum_k W_x(\omega_k, \tau) e^{i\omega_k \tau} (\Delta\omega_k) \\
&= (E_g)^{-1} \sum_l SW_x(\widetilde{\omega}_l, \tau) \Delta\widetilde{\omega}.
\end{aligned} \tag{13}$$

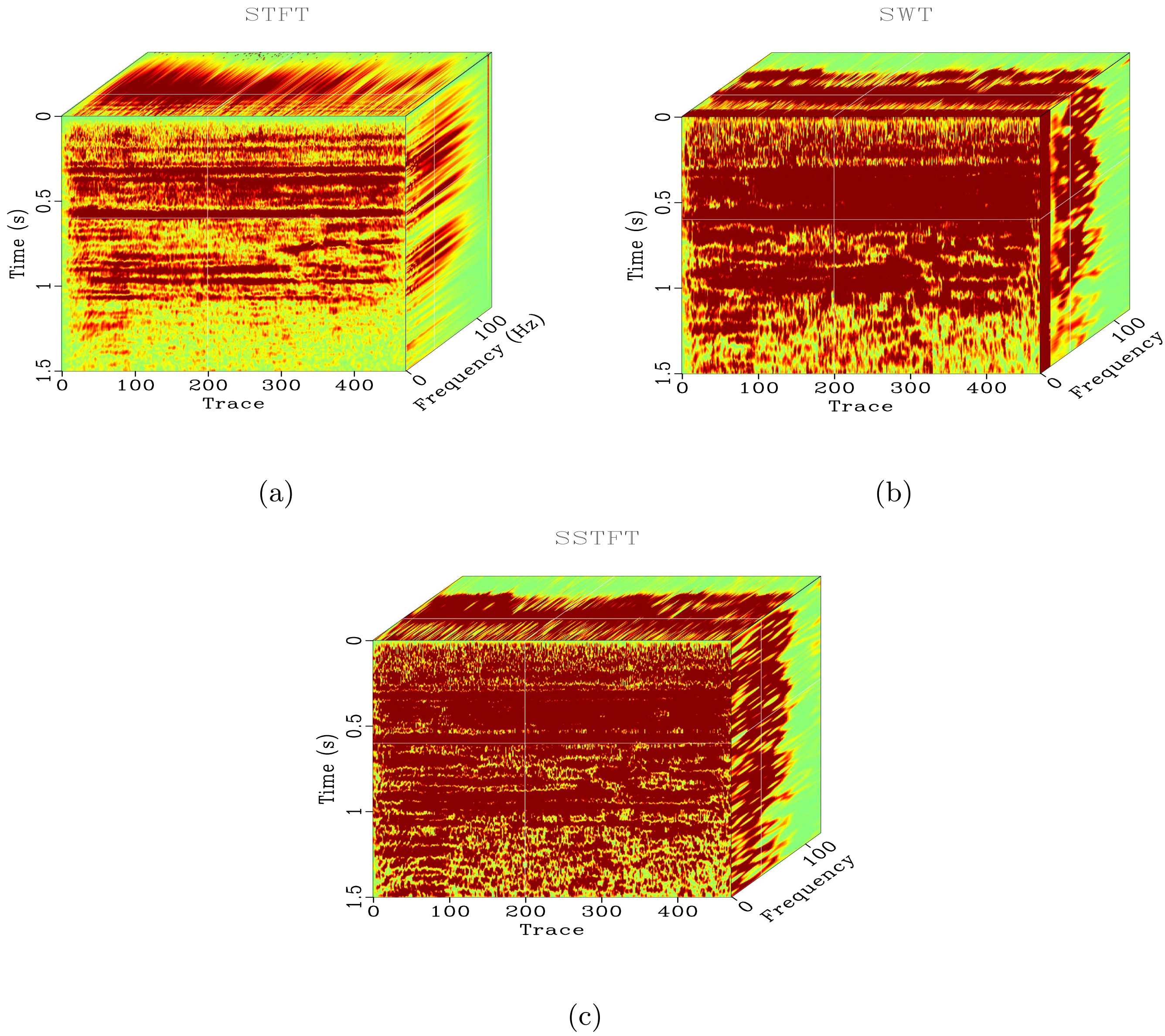

Figure 12. Time–frequency cubes for the real data of figure 11: (a) time–frequency using local attribute. (b) Time–frequency using SWT, with a 64-point length Morlet wavelet. (c) Time–frequency using SSTFT, with a 64-point length Gaussian window.

Relations with Oberlin's Fourier based synchrosqueezing transform

We underline the difference between the proposed method and Oberlin's Fourier based synchrosqueezing transform (Oberlin *et al* 2014).

The Oberlin's method has a threshold γ, the values of the STFT greater than the threshold can pass. The proposed method uses all the values of the STFT.

The compressing windows of the Oberlin's method are δ dependent, which usually are the Gaussian windows. The proposed method uses rectangle windows, which are constant.

The inversion of the Oberlin's method is incomplete, some data may have been removed by the threshold. The inversion of the proposed method is complete since it uses all the data.

Examples

Synthetic signals and real field data are used to test the proposed method.

Benchmark examples

Firstly, a simple synthetic signal is used to test the proposed method. Figure 1 is a synthetic signal $s(t)$, which consists of three components $s_1(t)$, $s_2(t)$, $s_3(t)$ as displayed in figure 2.

$$
\begin{aligned}
s(t) &= s_1(t) + s_2(t) + s_3(t),\\
s_1(t) &= (2 + 0.5\cos(2\pi t)) \times \cos(10\pi t)\\
s_2(t) &= \mathrm{e}^{-0.001t} \times \cos(40\pi t - 2.0t^2)\\
s_3(t) &= (2 + 0.5\cos(t)) \times (60\pi t + \sin(2\pi t)).
\end{aligned} \tag{14}
$$

The SWT (Daubechies *et al* 2011), and the local attribute method (Liu *et al* 2011), are used for comparative analyses. The

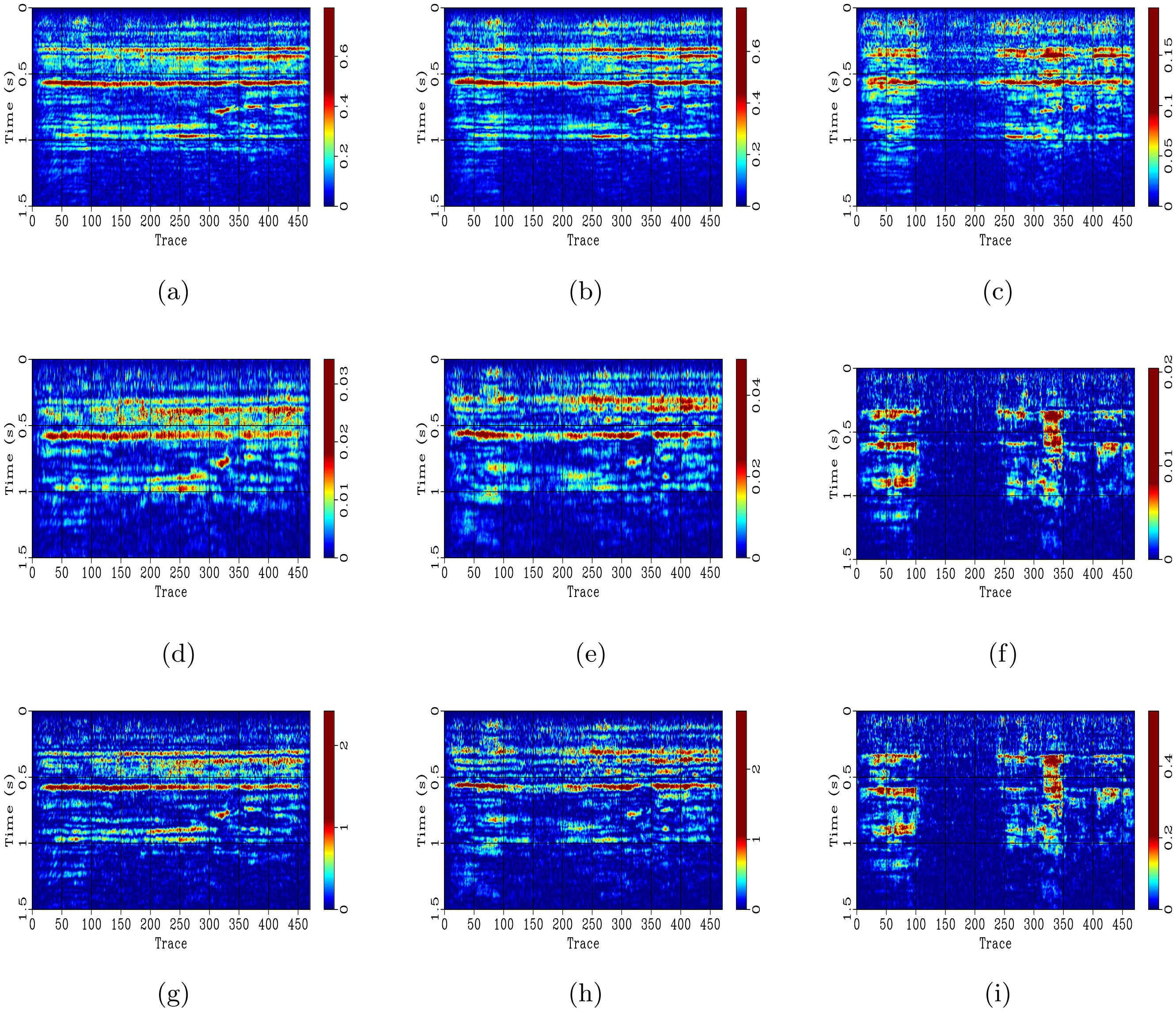

Figure 13. Constant slices for the real data of figure 11. Local attribute method: (a) 20 Hz. (b) 30 Hz. (c) 50 Hz. SWT method: (d) 20 Hz. (e) 30 Hz. (f) 50 Hz. SSTFT method: (g) 20 Hz. (h) 30 Hz. (i) 50 Hz.

local attribute method is a non-stationary time–frequency method. Figure 3(a) is the time–frequency map using local attribute method for the synthetic signal of figure 1. The time–frequency representations of SWT and SSTFT for the synthetic signal are displayed respectively in figures 3(b) and (c). For the SWT method, a 64-point length Morlet wavelet was used. For the SSTFT method, a 64-point length Gaussian window was used. From the figures, we see that the energies spread over the instantaneous frequencies locations for the local attribute method. The SSTFT and the SWT methods squeeze the energies to the instantaneous frequencies locations.

Figure 4 is another synthetic signal used by (Hou and Shi 2013). The signal consists of three components with variable frequencies and amplitudes. Figure 5(a) is the time–frequency representation using local attribute method. Figures 5(b) and (c) are time–frequency representations using respectively the SWT and the proposed method. All three methods correctly identify the three components. The proposed SSTFT method squeezes the time–frequency energies to the instantaneous frequencies locations, which make a concentrated time–frequency map.

Figure 6 is a 400 samples long recording of a bat chirp sampled with a sampling period 7 μs. This gives a sampling rate of 143 kHz. Figures 7(a)–(c) are the time–frequency representations using STFT, with a 64-point length Gaussian window, the Oberlin's synchrosqueezing STFT method (Oberlin *et al* 2014), with a 64-point Gaussian window and the proposed method with a 64-point Gaussian window. From the figures, we see that the bat chirp signal consists of three separated components. The Oberlin's synchrosqueezing method cannot reveal the high-frequency component.

The last example is a single seismic trace from a marine survey as displayed in figure 8. Figure 9(a) is the time–frequency map using local attribute method. The time–frequency representations of SSTFT and SWT for the trace are displayed respectively in figures 9(b) and (c). From the figures we see that the SSTFT and SWT methods squeeze the energies to the instantaneous frequencies locations. From the above figures,

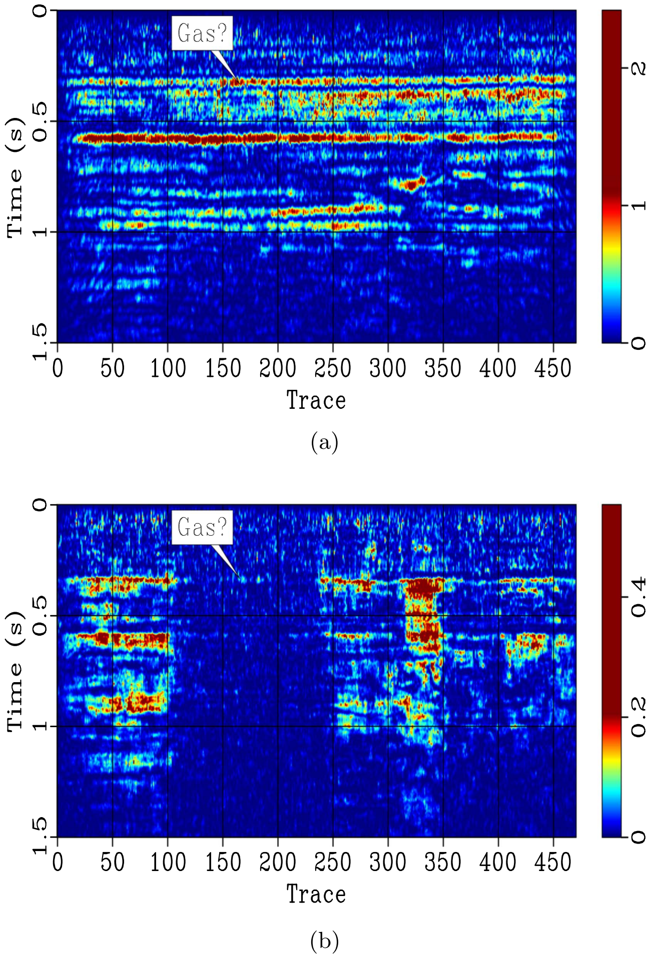

Figure 14. Constant slices for the real data of figure 11: (a) 20 Hz slice of SSTFT. (b) 50 Hz slice of SSTFT.

we can see that the energies for the SWT and SSTFT methods are not smoothly distributed due to the synchrosqueezing process. A local Gaussian smooth operator could be implemented to smooth the roughness.

Figure 10 shows the errors of reconstruction. The blue line is the reconstruction error for SWT method, and the red line is the error for SSTFT method. Both lines prove that the two methods are capable of reconstructing the original signal while keeping a small error.

Real data

Figure 11 is a 2D section from a land survey previously analyzed by Fomel (2007) and Liu *et al* (2011). Figures 12(a)–(c) are the time–frequency cubes using respectively local attribute method, SWT method, and SSTFT method. The front panels for the three cubes are the 40 Hz constant slices, the right panels are the 200th trace time–frequency maps, and the top panels are 0.6 s time depth time–frequency maps. All the three methods reveal the time-dependent frequency response of the seismic data. For the local attribute method (Liu *et al* 2011), the deep layers have week signals, whereas, for the SWT and SSTFT methods have relatively strong signals for the deep layers. The time–frequency response of local attribute method is mainly concentrated on the strong reflection layers, whereas, the time–frequency response are blended together for the SWT and SSTFT methods. We then extract the 20, 30 and 50 Hz constant slices for the three different methods mentioned above. Figures 13(a)–(c) are the 20, 30 and 50 Hz slices for local attribute method, figures 13(d)–(f) are the 20, 30 and 50 Hz slices for SWT method, and figures 13(g)–(i) are the 20, 30 and 50 slices for SSTFT method. From these 20 and 30 Hz constant slices, we see the energies are more concentrated for SSTFT and local attribute methods than the SWT method. However, for the 50 Hz constant slices, the energies are more concentrated for the local attribute method than those of the SWT and SSTFT methods.

Low-frequency anomalies can be used as hydrocarbon indicators, which may be attributed to the abnormal high-frequency attenuation in the gas filled reservoirs (Castagna *et al* 2003). The mechanisms for low-frequency anomalies of hydrocarbon reservoirs are still not clearly understood (Ebrom 2004, Kazemeini *et al* 2009). Figures 14(a) and (b) are the 20 and 50 Hz constant slices of the SSTFT method. Comparing the slices, a low-frequency anomaly in the top-left part of the section is apparent indicated by the text box, which might be viewed as an indicator of the gas presentation (Castagna *et al* 2003).

Conclusions

SSTFT is a concentrated version of the STFT, which improves the time–frequency resolution of the STFT by synchrosqueezing method. Since seismic signals are non-stationary, the proposed method can be used as a tool for spectral anomalies detection, and thus improves the prediction of oil and gas reservoirs. Further applications include image processing, de-nosing etc.

Acknowledgments

Our deepest gratitude goes to the anonymous reviews for their careful work and thoughtful suggestions that helped improve this paper substantially. We would like to thank E Bredo for his Matlab Synchrosqueezing Toolbox. The Madagascar open source software package is such a great platform that helped us to conduct meaningful research efficiently, which will be helpful in my future works. This work is partially supported by Science Foundations of China University of Petroleum (Grant No.2462015YQ0604).

Appendix. Synchrosqueezing wavelet transform

Synchrosqueezing wavelet transform was a special case of reassignment method (Chassande-Mottin *et al* 1997, Daubechies *et al* 2011, Auger *et al* 2013), which based on the wavelet transform with the aim of sharping the time–frequency map by reallocating the point of computation to the instantaneous frequency of the input signal. The continuous wavelet transform of a signal $x(t)$ is defined by (Mallat 2009)

$$W_x(a, b) = \int_{-\infty}^{\infty} x(t) a^{\frac{1}{2}} \overline{\psi\left(\frac{t-b}{a}\right)} \mathrm{d}t, \tag{A.1}$$

where $\overline{\psi}$ is the complex conjugate of a wavelet ψ, a is the scale variable, and b is the time location. Consider the purely harmonic signal $x(t) = A\cos(\omega t)$, whose Fourier transform is

$$\hat{x}(\xi) = A\pi[\delta(\xi - \omega) + \delta(\xi + \omega)]. \tag{A.2}$$

By Parseval's theorem (Mallat 2009), we can rewrite equation (A.1) as

$$W_x(a, b) = \frac{1}{2\pi} \int_{-\infty}^{\infty} \hat{x}(\xi) a^{\frac{1}{2}} \overline{\hat{\psi}(a\xi)} \mathrm{e}^{\mathrm{i}b\xi} \mathrm{d}\xi, \tag{A.3}$$

where ξ is the angular frequency. Suppose $\hat{\psi}$ is an analytical signal, its frequency contents are positive. Substituting equation (A.2) into (A.3) yields

$$W_x(a, b) = \frac{A}{2} a^{\frac{1}{2}} \overline{\hat{\psi}(a\omega)} \mathrm{e}^{\mathrm{i}b\omega}. \tag{A.4}$$

Daubechies *et al* (2011) pointed out that the instantaneous frequency can be computed for $\omega(a, b)$ with any (a, b) for which $W_x(a, b) \neq 0$ by

$$\omega(a, b) = -\mathrm{i} W_x(a, b)^{-1} \frac{\partial W_x(a, b)}{\partial b}, \tag{A.5}$$

the time-scale plane is translated to the time–frequency plane according to the map $(a, b) \to (a, \omega(a, b))$. If the discrete points for the continuous variables a and ω are taken a_k, $(\Delta a)_k = a_k - a_{k-1}$ and ω_l, $(\Delta\omega)_l = \omega_l - \omega_{l-1}$. We can get the synchrosqueezing wavelet transform based on the above assumption as (Daubechies *et al* 2011, Thakur *et al* 2013),

$$T_x(\omega_l, b) = (\Delta\omega)^{-1} \sum_{a_k: |\omega(a_k, b) - \omega_l| \leqslant \Delta\omega/2} W_x(a_k, b) a_k^{-\frac{3}{2}} (\Delta a)_k. \tag{A.6}$$

We then get the squeezed time–frequency representation by summing different contributions to the center frequency, which sharpen the time–frequency map. The following shows that the signal can be reconstructed after the synchrosqueezing. Assuming $C_\psi = \frac{1}{2}\int_0^\infty \overline{\hat{\psi}(\xi)} \frac{\mathrm{d}\xi}{\xi}$, the reconstruction equation is (Daubechies *et al* 2011),

$$x(b) = \Re\left[C_\psi^{-1} \int_0^\infty W_x(a, b) a^{\frac{-3}{2}} \mathrm{d}a\right], \tag{A.7}$$

where $\Re$ takes the real part of a complex number. The discrete reconstruction formula is (Daubechies *et al* 2011),

$$\begin{aligned} x(b) &\approx \Re\left[C_\psi^{-1} \sum_k W_x(a_k, b) a_k^{\frac{-3}{2}} (\Delta a)_k\right] \\ &= \Re\left[C_\psi^{-1} \sum_l T_x(\omega_l, b)(\Delta\omega)\right]. \end{aligned} \tag{A.8}$$

ORCID iDs

Guoning Wu https://orcid.org/0000-0003-2155-9738

References

Auger F, Chassande-Mottin E and Flandrin P 2012 Making reassignment adjustable: the Levenberg–Marquardt approach *Proc. IEEE-ICASSP* pp 3889–92
Auger F and Flandrin P 1995 Improving the readability of time–frequency and time-scale representations by reassignment method *IEEE Trans. Signal Process.* **43** 1068–89
Auger F, Flandrin P and Lin Y T 2013 Time-frequency reassignment and synchrosqueezing: an overwiew *IEEE Signal Process.* **30** 32–41
Castagna J, Sun S and Siegfried R W 2003 Instantaneous spectral analysis: detection of low-frequency shadows associated with hydrocarbons *Leading Edge* **22** 120–7
Chassande-Mottin E, Daubechies I, Auger F and Flandrin F 1997 Differential reassignment *IEEE Signal Process. Lett.* **4** 293–4
Chen Y, Liu T, Chen X, Li J and Wang E 2014 Time-frequency analysis of seismic data using synchrosqueezing wavelet transform *J. Seismic Explor.* **23** 303–12
Cohen L 1989 Time–frequency distributions—a review *Proc. IEEE* **77** 941–81
Daubechies I, Lu J and Wu H T 2011 Synchrosqueezed wavelet transforms: an empirical mode decomposition-like tool *Appl. Comput. Harmon. Anal.* **30** 243–61
Ebrom D 2004 The low frequency gas shadows in seismic sections *Leading Edge* **23** 772
Fomel S 2007 Shaping regularization in geophysical-estimation problems *Geophysics* **72** R29–36
Herrera R, Han J and der Baan M 2014 Application of the synchrosqueezing transform in seismic time–frequency analysis *Geophysics* **79** V55–64
Holighaus N, Prusa Z and Sondergaard P 2016 Reassignment and synchrosqueezing for general time–frequency filter banks, subsampling and processing *Signal Process.* **125** 1–8
Hou T Y and Shi Z 2013 Data-driven time–frequency analysis *Appl. Comput. Harmon. Anal.* **35** 284–308
Huang N E, Shen Z, Long S R, Wu M C, Shih H H, Zheng Q, Yen N C, Tung C C and Liu H H 1998 The empirical mode decomposition and the Hilbert spectrum for nonlinear and non-stationary time series analysis *Proc. R. Soc.* A **454** 903–95
Huang Z, Zhang J, Hu Zhao T and Sun Y 2015 Synchrosqueezing S-transform and its application in seismic spectral decomposition *IEEE Trans. Geosci. Remote Sens.* **54** 817–25
Huang Z, Zhang J and Zou Z 2017 A second-order synchrosqueezing S-transform and its application in seismic spectral decomposition *Chin. J. Geophys.* **60** 627–39
Huang Z H, Zhang J Z, Zhao T H and Sun Y B 2016 Synchrosqueezed S-transform and its application in seismic spectral analysis *IEEE Trans. Geosci. Remote Sens.* **54** 717–825
Kazemeini S H, Juhlin C, Jorgensen K Z and Norden B 2009 Application of the continuous wavelet transform on seismic data for mapping of channel deposits and gas detection at the CO2SINK site, Ketzin, Germany *Geophys. Prospect.* **57** 111–23
Liu G, Fomel S and Chen X 2011 Time–frequency analysis of seismic data using local attributes *Geophysics* **76** P23–34
Liu W, Cao S and Chen Y 2016 Seismic time–frequency analysis via empirical wavelet transform *IEEE Geosci. Remote Sens. Lett.* **13** 28–32

Mallat S 2009 *A Wavelet Tour of Signal Processing: The Sparse Way* (New York: Academic)

Mallat S G 1989 A theory for multiresolution signal decomposition: the wavelet representation *IEEE Trans. Pattern Anal. Mach. Intell.* **11** 674–93

Oberlin T, Meignen S and Perrier V 2014 The Fourier-based synchrosqueezing transform *Proc. IEEE Int. Conf. Acoust. Speech Signal Process* pp 315–9

Oberlin T, Meignen S and Perrier V 2015 Second-order synchrosqueezing transform or invertible reassignment? Towards ideal time–frequency representations *IEEE Trans. Signal Process.* **63** 1335–44

Reine C, van der Baan M and Clark R 2009 The robustness of seismic attenuation measurements using fixed- and variable-window time-frequency transforms *Geophysics* **74** 123–35

Stockwell R G, Mansinha L and Lowe R P 1996 Localization of the complex spectrum *IEEE Trans. Signal Process.* **44** 998–1001

Tary J B, Herrera R H, Han J and van der Baan M 2014 Spectral estimation-What is new? What is next? *Rev. Geophys.* **52** 723–49

Thakur G, Brevdo E, Fuckar N S and Wu H T 2013 The synchrosqueezing algorithm for time-varying spectral analysis: robustness properties and new paleoclimate application *Signal Process.* **93** 1079–94

Torres M E, Colominas M A, Schlotthauer G and Flandrin P 2011 A complete ensemble empirical mode decomposition with adaptive noise *IEEE Int. Conf. on Acoustics, Speech and Signal Processing (ICASSP)* (Piscataway, NJ: IEEE) pp 4144–7

Wang S, Chen X, Tong C and Zhao Z 2016 Matching synchrosqueezing wavelet transform and application to aeroengine vibration monitoring *IEEE Trans. Instrum. Meas.* **66** 1–13

Wang S, Chen X, Wang Y, Cai G, Ding B and Zhang X 2015 Nonlinear squeezing time–frequency transform for weak signal detection *Signal Process.* **113** 195–210

Wu Z and Huang N E 2009 Ensemble empirical mode decomposition: a noise-assisted data analysis method *Adv. Adapt. Data Anal.* **1** 1–41